

Article

ZIF-67(Co)-Loaded Filter Paper for In Situ Catalytic Degradation of Bisphenol A in Water

Zhimin Cai ¹, Yutao Luo ¹ and Lu Gan ^{2,3,*}¹ College of Economics and Management, Nanjing Forestry University, Nanjing 210037, China² College of Materials Science and Engineering, Nanjing Forestry University, Nanjing 210037, China³ Jiangsu Co-Innovation Center of Efficient Processing and Utilization of Forest Resources, International Innovation Center for Forest Chemicals and Materials, College of Materials Science and Engineering, Nanjing Forestry University, Nanjing 210037, China

* Correspondence: ganlu@njfu.edu.cn

Abstract: Herein, we loaded cobalt-based zeolite imidazolate frameworks, ZIF-67 (Co), onto commercial filter paper to prepare catalytic filter paper (ZFP) for the in situ degradation of bisphenol A (BPA) in water by activating peroxymonosulfate. The results showed that ZIF-67 (Co) was densely and uniformly distributed on the surface of the filter paper. The prepared ZFP could effectively degrade BPA in situ through a gravity-driven filtration process. Specifically, when the flow rate of the BPA solution passing through ZFP was lower than 10 mL/min, 0.02 mM of BPA could be completely degraded by ZFP. Furthermore, ZFP showed promising water matrix adaptability, which could provide promising BPA degradation efficiency in a wide pH range or in the existence of multiple anions. The scavenging tests demonstrated that both sulfate radical and hydroxyl radical were generated for BPA degradation, in which hydroxyl radical was the dominant active species. The ZFP also exhibited promising long-time use stability with a high mineralization rate. This study provides a novel method to prepare high-efficient catalyst paper for the in situ organic pollutant removal in water media via a prompt filtration process.



Citation: Cai, Z.; Luo, Y.; Gan, L. ZIF-67(Co)-Loaded Filter Paper for In Situ Catalytic Degradation of Bisphenol A in Water. *Separations* **2022**, *9*, 340. <https://doi.org/10.3390/separations9110340>

Academic Editor: Piotr Paweł Wiczorek

Received: 9 October 2022

Accepted: 1 November 2022

Published: 3 November 2022

Publisher's Note: MDPI stays neutral with regard to jurisdictional claims in published maps and institutional affiliations.



Copyright: © 2022 by the authors. Licensee MDPI, Basel, Switzerland. This article is an open access article distributed under the terms and conditions of the Creative Commons Attribution (CC BY) license (<https://creativecommons.org/licenses/by/4.0/>).

Keywords: peroxymonosulfate; degradation; catalytic filter paper; zeolite imidazolate frameworks

1. Introduction

In recent decades, water contamination by organic pollutants has caused enormous threats to both the ecological environment and human health [1–3]. Among all the organic pollutants, endocrine-disrupting chemicals (EDCs) have received tremendous concern since EDCs can disrupt the endocrine system of human beings seriously if they are excessively accumulated in the internal organs [4]. Bisphenol A (BPA), a classic EDC that is commonly used in the chemical synthesis field, has been frequently detected in various water bodies, with concentrations exceeding the threshold of many national standards [5,6]. However, traditional wastewater treatment methods, including activated sludge process, adsorption, and flocculation processes, are not capable of separating BPA from water completely [7,8]. Thus, it is a great necessity to develop ways to remove BPA effectively.

Advanced oxidation processes (AOPs), including the photocatalytic process, the Fenton process, etc., are regarded as significant approaches for the removal of organic pollutants in water, in which sulfate radical-based (SO_4^-) AOPs are frequently selected since SO_4^- can degrade almost all the organic pollutants with a wide pH application range and long half-life period [9]. In general, SO_4^- can be generated by activating persulfate, including peroxymonosulfate (PMS) and/or peroxydisulfate (PDS), through various means [10]. Compared with heat, ultraviolet, ultrasound, and electrochemical approaches, transition-metal-based catalysts can promptly activate persulfate under ambient conditions with a high SO_4^- generation rate, in which the cobalt catalyst/PMS system is regarded as one of the most promising systems for SO_4^- generation and organic pollutant degradation [11].

Recently, cobalt-based metal–organic frameworks (MOFs) have been of particular interest as PMS-activating catalysts since MOFs have many promising characteristics such as controllable porosity, multiple functionalities, and high catalytic activity [12]. Compared with other Co-MOFs, zeolite imidazolate frameworks (ZIFs) such as ZIF-67(Co) are frequently selected since they have desirable chemical stability and synthesis simplicity [13]. Moreover, ZIF-67(Co) has been proven to be an efficient PMS activation agent for organic pollutant degradation [14].

Another concern of using the cobalt catalyst/PMS system for organic pollutant degradation is that the catalysts cannot readily be separated from the reaction solution after the degradation process is finished. It has been widely accepted that membrane filtration is an effective and easy-to-operate method for the purification of wastewater [15]. Thus, in the present study, ZIF-67(Co) is prepared and loaded on commercial filter paper to prepare catalytic filter paper. Since the catalyst was loaded in the filter matrix, the filter paper could immobilize the ZIF-67(Co) and had the potential to in situ degrade the BPA in the water when the BPA solution passed through the catalytic paper. Furthermore, the used catalytic paper could be readily recycled and reused, which avoided the introduction of secondary pollution to the water body like other powdery catalysts did. The impact of many parameters on the degradation performance of the catalytic paper is systematically studied. The active species in the reaction system are also elucidated.

2. Materials and Methods

2.1. Chemicals

Cobalt nitrate hexahydrate ($\text{Co}(\text{NO}_3)_2 \cdot 6\text{H}_2\text{O}$) and 2-methylimidazole ($\geq 99\%$) were purchased from Aladdin Chemical Co., Ltd. (Shanghai, China). BPA ($\geq 99\%$) and PMS (Oxone: KHSO_5 , 0.5KHSO_4 , $0.5\text{K}_2\text{SO}_4$) were purchased from Sigma-Aldrich Company (USA). Commercial qualitative filter paper ($d = 5$ cm) was purchased from Double Ring (China). Other reagents were of analytical grade and used as received without purification. Distilled water (H_2O) was obtained by the Hi-Tech water purification instrument.

2.2. Preparation of Catalytic Paper

ZIF-67(Co)-loaded catalytic paper (ZFP) was prepared by a precipitation method described as follows. Firstly, one piece of filter paper was immersed in 50 mL of methanol. Afterward, 500 mg of $\text{Co}(\text{NO}_3)_2 \cdot 6\text{H}_2\text{O}$ was added and dissolved. Then, 20 mL methanol solution containing 660 mg 2-methylimidazole was dropped into the above mixed solution gradually under slow magnetic stirring. The mixture was aged for 24 h, and ZIF-67(Co)-loaded filter paper with ~ 700 mg ZIF-67(Co) loading amount was obtained after being washed twice with methanol and then dried in an oven at 60°C for 12 h.

2.3. Characterizations

The morphology of the ZFP was observed by a scanning electron microscope (SEM, JEOL SEM 6490, Japan). An X-ray diffraction diffractometer (XRD, Rigaku Smartlab, Japan) was employed to analyze the crystalline structure of the ZFP. The thermogravimetric analysis of the composites was conducted with a TGA instrument (Mettler Toledo; TGA/DSC 1 Simultaneous Thermal Analyzer) from room temperature to 700°C and $5^\circ\text{C}/\text{min}$ under N_2 atmosphere. The concentration of the BPA was analyzed by high-performance liquid chromatography (HPLC, Dionex Ultimate 3000) equipped with a Thermo C18 column ($5\ \mu\text{m}$ particle size, 250×4.6 mm). The concentrations of dissolved Co ions in the solutions were also determined with atomic absorption spectroscopy (AAS, AA800, PerkinElmer). The total organic carbon (TOC) was measured by a MutiN/C 2100 analyzer.

2.4. Catalytic Degradation of BPA in ZFP/PMS System

The in situ degradation of BPA by ZFP was carried out by a gravity-induced filtration process, as illustrated in Figure 1. Specifically, the ZFP was put in a sand core filter ($d = 5$ cm) with a vacuum pump. Typically, 20 mL of BPA solution with a certain concentra-

tion and 0.3 mL of PMS (1.5 mM) solution were added into the filter, and the flow rate was adjusted from 2 mL/min to 20 mL/min (10 min to 1 min for 20 mL BPA of solution passing through the ZFP) by the vacuum pump with controllable negative pressure. A 1.0 mL volume of BPA solution passing through the ZFP was collected, filtered with a 0.22 μm polytetrafluoroethylene membrane, and immediately quenched with 0.5 mL methanol before analysis. The initial pH value of the solution was measured after PMS and catalyst were added and was adjusted by NaOH (1 M) and H₂SO₄ (1 M). Methanol (MeOH), isobutanol (TBA), and L-histidine were selected as scavengers for scavenging tests. The long-time use stability of the ZFP was tested by repeating the above BPA test for 5 consecutive runs, in which the flow rate was adjusted to be 5 mL/min. All the degradation tests were triplicated, and the data were the average values with standard deviations.

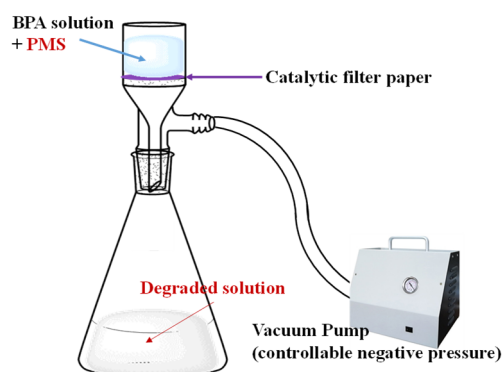


Figure 1. Schematic illustration of the BPA degradation by ZFP.

3. Results and Discussion

The morphology of the prepared ZFP was investigated in terms of SEM, with the results shown in Figure 2. As illustrated in Figure 2a, pristine ZIF-67(Co) had a polyhedral structure with uniform particle distributions. As for the ZFP shown in Figure 2b, it was seen that ZIF-67(Co) particles were densely and uniformly loaded on the surface of the filter paper, in which the ZIF-67(Co) also exhibited its pristine polyhedral morphology with smaller particle sizes. This might be because the commercial paper had a cellulose structure with abundant hydroxyl groups that could interact with ZIF-67(Co), resulting in a restraining effect on the growth of the ZIF-67(Co) on the filter paper surface. From the EDS mapping images shown in Figure 2b,c, it was seen that the Co element was uniformly distributed within the ZFP. Additionally, the EDS elemental analysis indicated that C, N, O, and Co occupied 58.96 wt%, 6.61 wt%, 6.46 wt%, and 27.97 wt% in the ZFP, indicating that there are enough active sites available for PMS activation.

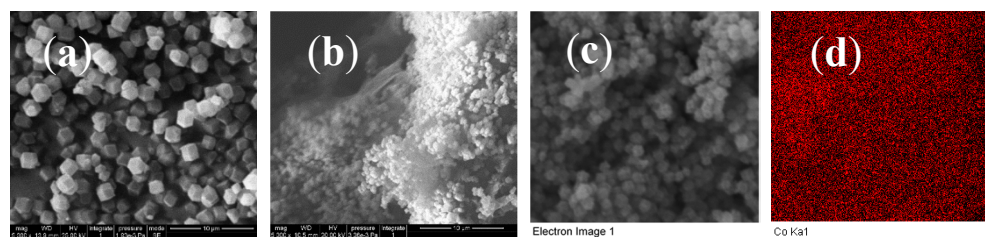


Figure 2. SEM images of (a) ZIF-67 and (b) ZFP (c) selected area and (d) EDS Co elemental mapping in ZFP.

The crystalline structure of the prepared ZFP was afterward studied using XRD, with the results shown in Figure 3a. It was seen that the unloaded filter paper had a main characteristic peak at 22.1°, which was associated with the (002) crystalline plane of the Cellulose I structure [16,17]. This meant the filter paper was composed of natural cellulose without post-treatment. At the same time, the prepared ZIF-67(Co) had multiple shape peaks,

which were all assigned to the characteristic peaks of the cobalt-based ZIF structure [18]. After ZIF-67(Co) was loaded on the filter paper, the resulting ZFP exhibited a similar XRD pattern with ZIF-67(Co), and the pattern of filter paper was not observed. This was probably because the sharp peaks of large amounts of ZIF-67(Co) particles shielded the broad diffraction peaks of the filter paper with comparatively weak intensity. The TGA of the ZFP conducted under N₂ atmosphere is shown in Figure 3b. As illustrated, the ZFP began to decompose when the temperature increased to ~300 °C, which was ascribed to the decomposition of the lignocellulose component in the filter paper and the organic ligand in ZIF-67(Co) [19]. When the temperature increased to 500 °C, the weight loss gradually ceased, indicating that the organic compounds and polymers were converted to carbonaceous materials. Figure 3c shows the N₂ adsorption/desorption curves for the pristine filter paper and the ZFP. It was found that since ZIF-67(Co) was porous material with rich porosity, the loading of ZIF-67(Co) significantly increased the surface area of the pristine filter paper.

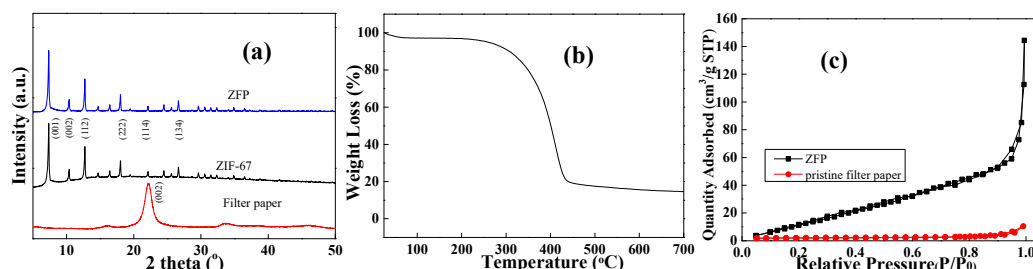


Figure 3. (a) XRD patterns of the prepared samples; (b) TGA and (c) N₂ adsorption/desorption curves of ZFP.

The catalytic degradation performance of the ZFP was then investigated by degrading BPA in water. Figure 4a shows the in situ BPA removal efficiency after the BPA solution with different flow rates passed through the ZFP. It is shown from the inset figure of Figure 4a that 0.2 g/L of pristine ZIF-67(Co) could completely degrade 0.02 mM BPA within 15 min. When ZIF-67(Co) was loaded on the filter paper, the resulting ZFP also exhibited high BPA removal efficiency. Furthermore, the lower flow rate of the solution facilitated the BPA degradation. When the flow rate of BPA decreased to lower than 10 mL/min, 0.02 mM of the BPA in the solution could be completely degraded after the solution passed through the ZFP. This was because ZIF-67(Co) had a higher possibility to contact with PMS and generate more active species at a lower flow rate.

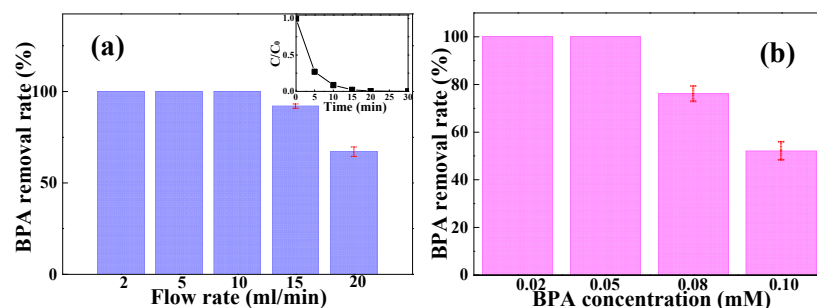


Figure 4. Impact of (a) solution flow rate (inset: catalytic performance of ZIF-67(Co) (0.2 g/L) toward BPA (0.02 mM) degradation) and (b) BPA concentration on the catalytic performance of ZFP.

The impact of BPA concentration on the performance of the ZFP was then investigated, in which the solution flow rate was fixed at 5 mL/min. As illustrated in Figure 4b, increased BPA concentration inhibited the performance of the ZFP since active species with a fixed generation speed were not capable of degrading the increased number of BPA molecules in the solution. It was still investigated that the ZFP could completely degrade the BPA in

the solution when the concentration of the BPA was lower than 0.05 mM, indicating the promising in situ catalytic capability of the ZFP.

The in situ BPA degradation performance of the ZFP at different water conditions was then investigated, with the results shown in Figure 5, in which the solution flow rate was fixed at 5 mL/min, and the BPA concentration was set at 0.02 mM. Figure 5a shows the impact of the solution pH value on the performance of the ZFP. It was seen that the BPA degradation efficiency fluctuated with the change in the solution pH, which indicated that active species mainly dominated the BPA degradation in the reaction system. Meanwhile, the acidic condition was beneficial for the BPA degradation, which reflected the nature of the Fenton-like reactions [20]. When the pH value increased to basic conditions, the activity of the ZFP increased, and the BPA degradation efficiency reached a peak at the pH value of 9, since the generated SO_4^- could contact with more hydroxyl ions (OH^-) to produce hydroxyl radicals (OH) [21]. When further increasing the pH value to 11, excessive OH^- would inhibit the contact between the ZFP and the PMS, resulting in the decline of the ZFP activity [22].

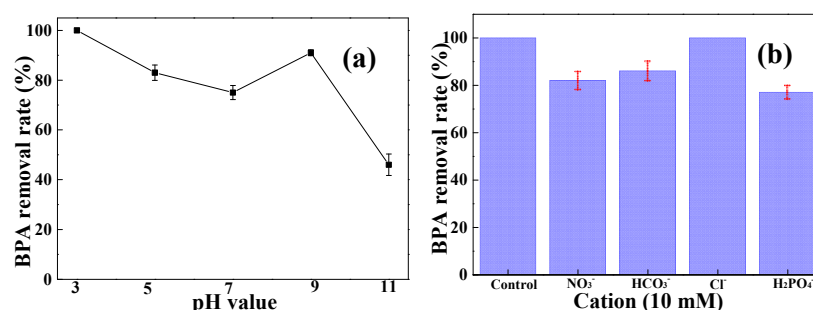


Figure 5. Impact of (a) pH value and (b) anions on the catalytic performance of ZFP ($[\text{BPA}]_0 = 0.02 \text{ mM}$, flow rate = 5 mL/min).

Figure 5b shows the impact of different anions on the performance of the ZFP. As illustrated, all the introduced anions obviously inhibited the activity of the ZFP except Cl^- . This was because Cl^- could react with OH in the solution and generate abundant chlorine-based active species such as Cl and ClOH^- , which also took part in the BPA degradation [23]. Otherwise, the foreign anions would either occupy the active sites on the ZFP or compete with the BPA for active species consumptions, which both had a negative impact on the ZFP performance toward the BPA degradation [24].

The generated active species that dominated the BPA degradation in the ZFP/PMS system were analyzed through scavenging tests. Table 1 summarizes the BPA degradation rate in the ZFP/PMS system at the existence of various scavengers. It was first observed that L-histidine did not show an inhibition effect on the ZFP performance, indicating that non-radical active species were not generated in the reaction system. Meanwhile, both methanol and t-butyl alcohol had a significant quenching effect on the BPA degradation [25]. This indicated that the BPA degradation was dominated by the radical species. Methanol was an effective quencher for both OH ($k_{\bullet\text{OH}} = \sim 1.9 \times 10^9 \text{ M}^{-1}\text{s}^{-1}$) and SO_4^- ($k_{\text{SO}_4\bullet-} = \sim 2.6 \times 10^7 \text{ M}^{-1}\text{s}^{-1}$), whereas tert-butyl alcohol had a higher quenching activity to OH ($k_{\bullet\text{OH}} = \sim 6.2 \times 10^8 \text{ M}^{-1}\text{s}^{-1}$) than SO_4^- ($k_{\text{SO}_4\bullet-} = \sim 5.2 \times 10^5 \text{ M}^{-1}\text{s}^{-1}$) [26]. This meant both OH and SO_4^- were generated in the reaction system for BPA degradation, in which OH was the dominant radical.

Table 1. Impact of different scavengers on the performance of SZP ($[\text{BPA}]_0 = 0.02 \text{ mM}$, flow rate = 5 mL/min).

Degradation Rate (%)	Scavenger			
	Control	L-Histidine	Methanol	T-Butyl Alcohol
	100	100	0	34

The long-time use stability of the ZFP was then investigated through continuous BPA degradation cycles, with the results shown in Figure 6a. As shown, the ZFP provided promising recyclability, which could completely remove the BPA in the reaction system for five consecutive cycles. Based on the AAS results, the concentrations of the leached Co^{2+} for five cycles were all lower than $50 \mu\text{g/L}$, indicating the promising stability of the ZFP. Furthermore, the XRD pattern of the used ZFP (Figure 6b) indicated that ZIF-67(Co) in the ZFP still maintained its crystalline structure after recycling. This meant the prepared catalytic filter paper had wide application potential for the in situ removal of organic pollutants in water.

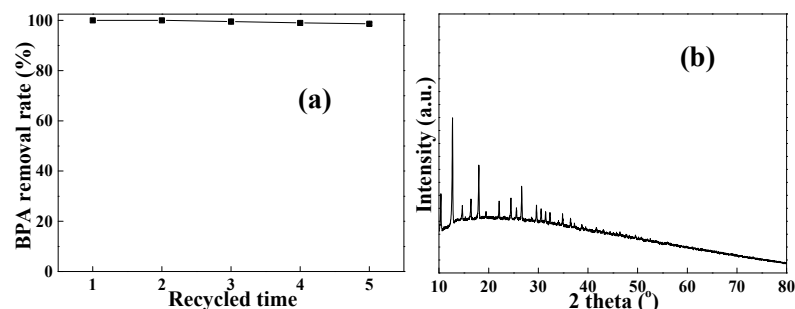


Figure 6. (a) Recyclability of ZFP ($[\text{BPA}]_0 = 0.02 \text{ mM}$, flow rate = 5 mL/min), (b) XRD pattern of recycled ZFP.

The TOC removal rate of BPA in the ZFP/PMS system was also investigated, with the results shown in Figure 7. It was shown that when BPA passed through the ZFP once, only 18% of the TOC was removed, which indicated that the degraded BPA molecules were only converted into degradation organic intermediates. Instead, when the degraded solution passed through the ZFP multiple times, the TOC removal rate would increase with the increase in the filtration times. When the BPA solution passed through the ZFP five times, more than 60% of the TOC could be removed. This was because the degradation intermediates could be further degraded by the radical active species to inorganic molecules such as CO_2 and H_2O if the pollutant and radical had a longer contact time. The TOC results indicated that the ZFP was a promising catalyst that could completely mineralize inorganic pollutants without introducing toxic degradation intermediates into the reaction solution.

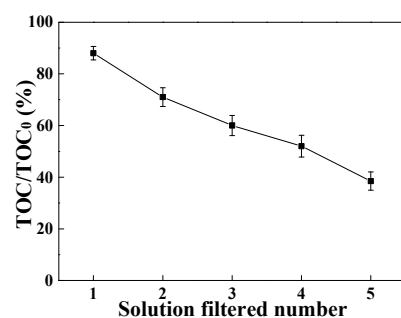


Figure 7. TOC removal of BPA in ZFP/PMS system ($[\text{BPA}]_0 = 0.02 \text{ mM}$, flow rate = 5 mL/min).

4. Conclusions

To conclude, ZFP was prepared in this study by loading ZIF-67(Co) onto the surface of commercial filter paper. The ZFP/PMS system exhibited promising in situ BPA degradation performance as a gravity-driven filter. A 0.02 mM amount of BPA could be completely degraded after passing through ZFP at the rate of 10 mL/min or lower. The ZFP also exhibited promising water matrix adaptability, which exhibited high BPA degradation efficiency at a wide pH application range and at the existence of various foreign anions. Additionally, the ZFP also provided excellent long-time use stability with a high TOC removal rate. Compared with previously reported studies, which frequently utilized

powdery catalysts for PMS activation, this study provides a new catalytic filter for the convenient removal of organic pollutants in water without introducing secondary pollution to the water media.

Author Contributions: Writing—original draft preparation, methodology, investigation, Z.C.; formal analysis, data curation, Y.L.; writing—review and editing, funding acquisition, project administration, L.G. All authors have read and agreed to the published version of the manuscript.

Funding: This research was funded by Natural Science Foundation of Jiangsu Province, China (BK20201385).

Data Availability Statement: Data are available upon request.

Acknowledgments: The Advanced Analysis and Testing Center of Nanjing Forestry University is acknowledged.

Conflicts of Interest: The authors declare no conflict of interest.

References

1. You, W.; Liu, L.; Xu, J.; Jin, T.; Fu, L.; Pan, Y. Effect of Anions and Cations on Tartrazine Removal by the Zero-Valent Iron/Peroxymonosulfate Process: Efficiency and Major Radicals. *Catalysts* **2022**, *12*, 1114. [\[CrossRef\]](#)
2. Pan, Y.; Qin, R.; Hou, M.; Xue, J.; Zhou, M.; Xu, L.; Zhang, Y. The interactions of polyphenols with Fe and their application in Fenton/Fenton-like reactions. *Sep. Purif. Technol.* **2022**, *300*, 121831. [\[CrossRef\]](#)
3. Yu, L.; Cheng, W.-x.; Wang, Q. The enhancement on biohydrogen production by the driving forces from extracellular iron oxide respiration. *Bioresour. Technol.* **2022**, *361*, 127679. [\[CrossRef\]](#)
4. Shi, J.; Dai, B.; Fang, X.; Xu, L.; Wu, Y.; Lu, H.; Cui, J.; Han, S.; Gan, L. Waste preserved wood derived biochar catalyst for promoted peroxymonosulfate activation towards bisphenol A degradation with low metal ion release: The insight into the mechanisms. *Sci. Total Environ.* **2022**, *813*, 152673. [\[CrossRef\]](#)
5. Xu, L.; Qi, L.; Han, Y.; Lu, W.; Han, J.; Qiao, W.; Mei, X.; Pan, Y.; Song, K.; Ling, C.; et al. Improvement of Fe²⁺/peroxymonosulfate oxidation of organic pollutants by promoting Fe²⁺ regeneration with visible light driven g-C₃N₄ photocatalysis. *Chem. Eng. J.* **2022**, *430*, 132828. [\[CrossRef\]](#)
6. Lu, H.; Gan, L. Catalytic Degradation of Bisphenol A in Water by Poplar Wood Powder Waste Derived Biochar via Peroxymonosulfate Activation. *Catalysts* **2022**, *12*, 1164. [\[CrossRef\]](#)
7. Wang, Z.; Jia, H.; Liu, Z.; Peng, Z.; Dai, Y.; Zhang, C.; Guo, X.; Wang, T.; Zhu, L. Greatly enhanced oxidative activity of δ-MnO₂ to degrade organic pollutants driven by dominantly exposed {−111} facets. *J. Hazard. Mater.* **2021**, *413*, 125285. [\[CrossRef\]](#)
8. Wang, Z.; Ju, C.; Zhang, R.; Hua, J.; Chen, R.; Liu, G.; Yin, K.; Yu, L. Acceleration of the bio-reduction of methyl orange by a magnetic and extracellular polymeric substance nanocomposite. *J. Hazard. Mater.* **2021**, *420*, 126576. [\[CrossRef\]](#)
9. Liu, C.; Liu, S.; Liu, L.; Tian, X.; Liu, L.; Xia, Y.; Liang, X.; Wang, Y.; Song, Z.; Zhang, Y.; et al. Novel carbon based Fe-Co oxides derived from Prussian blue analogues activating peroxymonosulfate: Refractory drugs degradation without metal leaching. *Chem. Eng. J.* **2020**, *379*, 122274. [\[CrossRef\]](#)
10. Ling, C.; Wu, S.; Dong, T.L.; Dong, H.F.; Wang, Z.X.; Pan, Y.W.; Han, J.G. Sulfadiazine removal by peroxymonosulfate activation with sulfide-modified microscale zero-valent iron: Major radicals, the role of sulfur species, and particle size effect. *J. Hazard. Mater.* **2022**, *423*, 127082. [\[CrossRef\]](#)
11. Liang, L.; Yue, X.; Dong, S.; Feng, J.; Sun, J.; Pan, Y.; Zhou, M. New insights into the effect of adsorption on catalysis in the metal-free persulfate activation process for removing organic pollutants. *Sep. Purif. Technol.* **2021**, *272*, 118923. [\[CrossRef\]](#)
12. Zhang, M.; Xiao, C.; Zhang, C.; Qi, J.; Wang, C.; Sun, X.; Wang, L.; Xu, Q.; Li, J. Large-Scale Synthesis of Biomass@MOF-Derived Porous Carbon/Cobalt Nanofiber for Environmental Remediation by Advanced Oxidation Processes. *ACS EST Eng.* **2021**, *1*, 249–260. [\[CrossRef\]](#)
13. Wu, Z.L.; Wang, Y.P.; Xiong, Z.K.; Ao, Z.M.; Pu, S.Y.; Yao, G.; Lai, B. Core-shell magnetic Fe₃O₄@Zn/Co-ZIFs to activate peroxymonosulfate for highly efficient degradation of carbamazepine. *Appl. Catal. B-Environ.* **2020**, *277*, 119136. [\[CrossRef\]](#)
14. Fang, X.; Gan, L.; Wang, L.; Gong, H.; Xu, L.; Wu, Y.; Lu, H.; Han, S.; Cui, J.; Xia, C. Enhanced degradation of bisphenol A by mixed ZIF derived CoZn oxide encapsulated N-doped carbon via peroxymonosulfate activation: The importance of N doping amount. *J. Hazard. Mater.* **2021**, *419*, 126363. [\[CrossRef\]](#)
15. Wu, Y.; Xu, L.; Shi, J.; Cui, J.; Han, S.; Xia, C.; Gan, L. Cobalt ferrite/cellulose membrane inserted catalytic syringe filter for facile in-situ filtration/degradation of emerging organic pollutants in water via activating peroxymonosulfate. *Mater. Design* **2022**, *220*, 110817. [\[CrossRef\]](#)
16. Zhao, Z.; Wu, D.; Huang, C.; Zhang, M.; Umemura, K.; Yong, Q. Utilization of enzymatic hydrolysate from corn stover as a precursor to synthesize an eco-friendly adhesive for plywood II: Investigation of appropriate manufacturing conditions, curing behavior, and adhesion mechanism. *J. Wood Sci.* **2020**, *66*, 85. [\[CrossRef\]](#)
17. Zhu, S.; Kumar Biswas, S.; Qiu, Z.; Yue, Y.; Fu, Q.; Jiang, F.; Han, J. Transparent wood-based functional materials via a top-down approach. *Prog. Mater. Sci.* **2023**, *123*, 101025. [\[CrossRef\]](#)

18. Zhuang, G.; Gao, Y.; Zhou, X.; Tao, X.; Luo, J.; Gao, Y.; Yan, Y.; Gao, P.; Zhong, X.; Wang, J. ZIF-67/COF-derived highly dispersed Co_3O_4 /N-doped porous carbon with excellent performance for oxygen evolution reaction and Li-ion batteries. *Chem. Eng. J.* **2017**, *330*, 1255–1264. [[CrossRef](#)]
19. Pan, Y.; Bu, Z.; Li, J.; Wang, W.; Wu, G.; Zhang, Y. Sulfamethazine removal by peracetic acid activation with sulfide-modified zero-valent iron: Efficiency, the role of sulfur species, and mechanisms. *Sep. Purif. Technol.* **2021**, *277*, 119402. [[CrossRef](#)]
20. Yang, X.; Biswas, S.K.; Han, J.; Tanpichai, S.; Li, M.-C.; Chen, C.; Zhu, S.; Das, A.K.; Yano, H. Surface and Interface Engineering for Nanocellulosic Advanced Materials. *Adv. Mater.* **2021**, *33*, 2002264. [[CrossRef](#)]
21. Bu, Z.; Li, X.; Xue, Y.; Ye, J.; Zhang, J.; Pan, Y. Hydroxylamine enhanced treatment of highly salty wastewater in $\text{Fe}^0/\text{H}_2\text{O}_2$ system: Efficiency and mechanism study. *Sep. Purif. Technol.* **2021**, *271*, 118847. [[CrossRef](#)]
22. Fang, X.; Wu, Y.; Xu, L.; Gan, L. Fast removal of bisphenol A by coconut shell biochar incorporated $\alpha\text{-MnO}_2$ composites via peroxymonosulfate activation. *J. Water Process Eng.* **2022**, *49*, 103071. [[CrossRef](#)]
23. Dong, X.; Ren, B.; Sun, Z.; Li, C.; Zhang, X.; Kong, M.; Zheng, S.; Dionysiou, D.D. Monodispersed CuFe_2O_4 nanoparticles anchored on natural kaolinite as highly efficient peroxymonosulfate catalyst for bisphenol A degradation. *Appl. Catal. B-Environ.* **2019**, *253*, 206–217. [[CrossRef](#)]
24. Wang, A.; Ni, J.; Wang, W.; Liu, D.; Zhu, Q.; Xue, B.; Chang, C.-C.; Ma, J.; Zhao, Y. MOF Derived Co–Fe nitrogen doped graphite carbon@crosslinked magnetic chitosan Micro–nanoreactor for environmental applications: Synergy enhancement effect of adsorption–PMS activation. *Appl. Catal. B-Environ.* **2022**, *319*, 121926. [[CrossRef](#)]
25. Gan, L.; Zhong, Q.; Geng, A.; Wang, L.; Song, C.; Han, S.; Cui, J.; Xu, L. Cellulose derived carbon nanofiber: A promising biochar support to enhance the catalytic performance of CoFe_2O_4 in activating peroxymonosulfate for recycled dimethyl phthalate degradation. *Sci. Total Environ.* **2019**, *694*, 133705. [[CrossRef](#)]
26. Zong, Y.; Guan, X.; Xu, J.; Feng, Y.; Mao, Y.; Xu, L.; Chu, H.; Wu, D. Unraveling the Overlooked Involvement of High-Valent Cobalt-Oxo Species Generated from the Cobalt(II)-Activated Peroxymonosulfate Process. *Environ. Sci. Technol.* **2020**, *54*, 16231–16239. [[CrossRef](#)]